nature structural & molecular biology

Crystal structure of the carnitine transporter and insights into the antiport mechanism

Lin Tang[1,3], Lin Bai[1–3], Wen-hua Wang[1] & Tao Jiang[1]

CaiT is a membrane antiporter that catalyzes the exchange of L-carnitine with γ-butyrobetaine across the *Escherichia coli* membrane. To obtain structural insights into the antiport mechanism, we solved the crystal structure of CaiT at a resolution of 3.15 Å. We crystallized CaiT as a homotrimer complex, in which each protomer contained 12 transmembrane helices and 4 L-carnitine molecules outlining the transport pathway across the membrane. Mutagenesis studies revealed a primary binding site at the center of the protein and a secondary substrate-binding site at the bottom of the intracellular vestibule. These results, together with the insights obtained from structural comparison with structurally homologous transporters, provide mechanistic insights into the association between substrate translocation and the conformational changes of CaiT.

Transporters are integral membrane proteins that catalyze the movement of ions or solutes across the membrane. These proteins can be classified into three types on the basis of the energy source used for transport: (i) primary active transporters, which use chemical energy (usually ATP) to translocate substrates; (ii) secondary active transporters, which use the electrochemical gradient of ions to transport a second substrate either along (symporter) or against (antiporter) the gradient; and (iii) precursor/product antiporters, which exchange one molecule with its metabolic product independently of ATP and the ion motive force[1,2]. Precursor/product antiporters are found in living cells, and they catalyze the exchange of various substrate pairs such as aspartate and glutamate, oxalate and formate, lactose and galactose, and ADP and ATP[3–6]. Studies have proposed that many membrane transporters operate via an 'alternating-access' mechanism in which the transporter switches between two major alternating conformations, inward facing and outward facing. In this process, the central binding site is alternately exposed to each side of the membrane, facilitating substrate translocation across the lipid bilayer[7–9]. However, because of the absence of structural data on substrate-bound precursor/product antiporters, there is little information on the detailed mechanism underlying precursor/product exchange, especially with respect to the number and structural characteristics of the substrate-binding sites. Furthermore, there is no definitive information on the process by which precursor and product binding trigger conformational changes.

Carnitine is a ubiquitous polar compound that is essential for the transport of activated fatty acids across the inner mitochondrial membrane, and carnitine deficiency causes critical metabolic disorders such as hypoglycemia, skeletal-muscle myopathy and cardiomyopathy[10–12]. Carnitine also plays important roles in various metabolic pathways in bacteria[13,14]. For example, in anaerobic growth conditions, some bacteria take up L-carnitine if no other electron acceptor or glucose is present and convert this carnitine into γ-butyrobetaine (4-trimethylaminobutyrate)[15]. To date, a number of carnitine transporters, including organic cation transporters in mammals[16–19] and CaiT[20] in bacteria, have been identified. CaiT in *E. coli* was identified as an L-carnitine/γ-butyrobetaine antiporter that belongs to the betaine/choline/carnitine transporter (BCCT) family, whose members transport substrates containing a quaternary ammonium group[20–22]. Functional studies revealed that the apparent affinity of CaiT for L-carnitine was about three times its affinity for D-carnitine and γ-butyrobetaine, whereas the binding affinities for acetyl-L-carnitine and glycine betaine were very weak[20]. The transport activity of CaiT has been studied by measuring carnitine uptake into proteoliposomes, and these studies indicated that CaiT shows similar catalytic activities in the exchange of L-carnitine/γ-butyrobetaine, L-carnitine/L-carnitine and L-carnitine/D-carnitine[20]. Moreover, unlike the other members of the BCCT family, all of which are Na^+- or H^+-dependent symporters, CaiT functions as a precursor/product antiporter independently of the ion gradient[23]. CaiT is also distinct from organic cation transporters, which are pH- or sodium-dependent transporters[16,17]. To obtain a better understanding of the transport mechanism of precursor/product antiporters, we determined the crystal structure of CaiT in the presence of its substrate L-carnitine.

RESULTS

Overall structure of CaiT

We solved the CaiT structure to a resolution of 3.15 Å by single-wavelength anomalous dispersion of a mercury derivative. The data-collection statistics and structure-determination information are summarized in **Table 1**. Each crystallographic asymmetric unit contains three CaiT molecules, which assemble into a homotrimer around a crystallographic

[1]National Laboratory of Biomacromolecules, Institute of Biophysics, Chinese Academy of Sciences, Beijing, China. [2]Graduate University of Chinese Academy of Sciences, Beijing, China. [3]These authors contributed equally to this work. Correspondence should be addressed to T.J. (tjiang@ibp.ac.cn).

Received 16 October 2009; accepted 17 February 2010; published online 28 March 2010; doi:10.1038/nsmb.1788

Table 1 Data collection and refinement statistics

	CaiT–L-carnitine
Data Collection	
Space group	$P6_3$
Cell dimensions	
a, *b*, *c* (Å)	134.2, 134.2, 85.1
α, β, γ (°)	90.0, 90.0, 120
Resolution (Å)	15–3.15 (3.32–3.15)[a]
R_{merge}	0.070 (0.391)
$I / \sigma I$	17.5 (4.4)
Completeness (%)	99.1 (98.2)
Redundancy	7.3 (5.4)
Refinement	
Resolution (Å)	15–3.15 (3.32–3.15)
No. reflections	14,327
R_{work}/ R_{free}	0.262 / 0.281
No. atoms	
Protein	3,903
Ligand	36
B-factors	
Protein	63.9
Ligand	59.5
R.m.s. deviations	
Bond lengths (Å)	0.013
Bond angles (°)	1.47

[a]Values in parentheses refer to data in the highest resolution shell.

threefold axis perpendicular to the membrane plane (**Supplementary Fig. 1**). This observation is consistent with previous biochemical data, including the data from native electrophoresis, cross-linking and gel filtration, which indicated that CaiT is a trimer in the detergent solution as well as in the cell membrane[24]. The CaiT monomer contains 12 transmembrane helical segments (TM1–TM12) with both the N and C termini exposed to the cytoplasm; thus, the monomer resembles a cylinder with a maximum height of ~52 Å and a maximum diameter of ~45 Å (**Fig. 1**). TM3–TM12 of CaiT form a structural core similar to the core of the Na^+-coupled symporter BetP[25] and the cores of the unrelated transporters LeuT[26], vSGLT[27], Mhp1 (ref. 28), AdiC[29,30] and ApcT[31]. In the structural core, TM3–TM7 and TM8–TM12 share a pseudo–two-fold rotation axis in the plane of the membrane. The r.m.s. deviation in the superimposition of the Cα traces of the 130 residues that constitute helices TM3–TM7 and TM8–TM12 is ~3 Å. The central group of four helices (TM3, TM4, TM8 and TM9) is stabilized by eight supporting transmembrane helices and one curved helix (H7). H7 is responsible for most of the direct interactions at the trimer interface (**Supplementary Fig. 1b**). The hydrogen bonding pattern in the TM3 helix shows a discontinuity around residues 100–102; this discontinuity divides the helix into intracellular (TM3i) and extracellular (TM3e) segments of approximately equal length. TM4 also shows a discontinuity at the middle region (around residues 143 and 144) (**Fig. 1** and **Supplementary Fig. 2**). The first two transmembrane helices, TM1 and TM2, flank the outer surfaces of TM11 and TM12 and form numerous contacts with TM4, TM8, TM9, TM11 and TM12.

Most of the transporters with solved structures and core topology similar to that of CaiT show either outward-facing or inward-facing conformations, with a cavity in the periplasmic or cytoplasmic side of the membrane. In a recent study, the Na^+-coupled symporter BetP was shown to adopt a conformation intermediate between the outward-facing conformation of LeuT and the inward-facing conformation of vSGLT, and this symporter contained one substrate in the 'occluded' central pocket. In the electron-density maps of the CaiT crystals with L-carnitine molecules, the CaiT monomer adopts an intermediate conformation similar to that of BetP, but the central binding site is open to the cytoplasmic side rather than being in the occluded conformation observed in BetP. Structural comparison reveals that CaiT is lacking a ~45-residue C-terminal helical extension observed in BetP; however, TM1–TM12 of CaiT superimpose well on BetP, with an r.m.s. deviation of ~2.3 Å. Furthermore, on the basis of the shape and size of nonprotein electron-density regions as well as the protein-substrate coordinations, we determined four L-carnitine molecules (LC-I–LC-IV) to be present along the substrate-translocation pathway[32] (**Fig. 2** and **Supplementary Fig. 3**).

Primary substrate-binding site

The first L-carnitine molecule (LC-I) is located in a cytoplasm-facing cavity near the unwound regions of TM3 and adjacent to the bent region of TM8. This binding site is located at a position equivalent to the substrate-binding sites in the structures of LeuT[26] (PDB 3F3E), vSGLT[27] (PDB 3DH4), Mhp1[28] (PDD 2JLO) and BetP[25] (PDB 2WIT); therefore, it is considered as the primary binding site (named S_{cen}) for the substrates (**Fig. 3**). LC-I is stabilized by cation-π interactions with Trp142 (TM4e) and Trp323 (TM8) and by hydrogen bonding interactions with Trp324 (TM8) (**Fig. 2b**). We induced two missense mutations around this site (W323L and W324L) and measured the uptake of [^{14}C]carnitine in proteoliposomes reconstructed with wild-type and mutated CaiT by performing a previously established transport assay[20]. Our results indicate that W323L and W324L mutations nearly abolished the transport activity (**Fig. 4**), suggesting that this binding site is essential in the transport cycle. In addition, we observed numerous aromatic-aromatic interactions around this substrate-binding pocket. On the extracellular side, a cluster of aromatic residues, including Tyr107, Tyr115, Trp142, Phe312, Trp316, Phe319, Tyr320, Trp323 and Trp363, as well as a nonaromatic residue, Glu111, formed a 12-Å-thick periplasmic hydrophobic barrier (**Fig. 3a**,**c**). The side chain carboxyl group of Glu111, which is conserved among the BCCT family members, was coordinated by the indole-ring nitrogen atoms of Trp142 and Trp363 and the side chain hydroxyl oxygen atoms of Tyr115 and Tyr320.

Secondary substrate-binding site

The second L-carnitine molecule, LC-II, is at the base of the intracellular vestibule, which is located ~6 Å from LC-I, and it forms cation-π interactions with Tyr327 (TM8) and hydrogen bonding interactions with Gln330 (TM8) (**Fig. 2c**), suggesting the existence

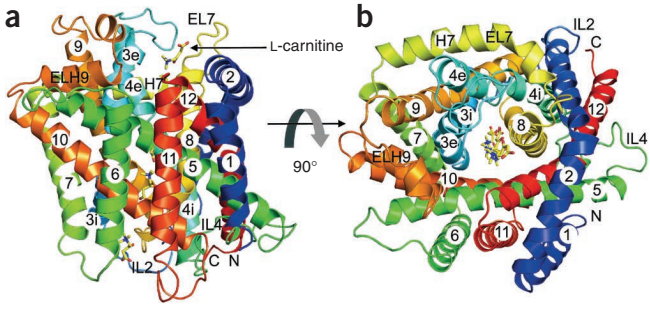

Figure 1 The overall structure of CaiT. (**a**) A ribbon diagram of the overall structure of CaiT, viewed parallel to the plane of the membrane. (**b**) The CaiT structure viewed from the periplasmic side. Four bound L-carnitine molecules are shown using a stick model. All three-dimensional illustrations in this manuscript were prepared using PyMOL[36].

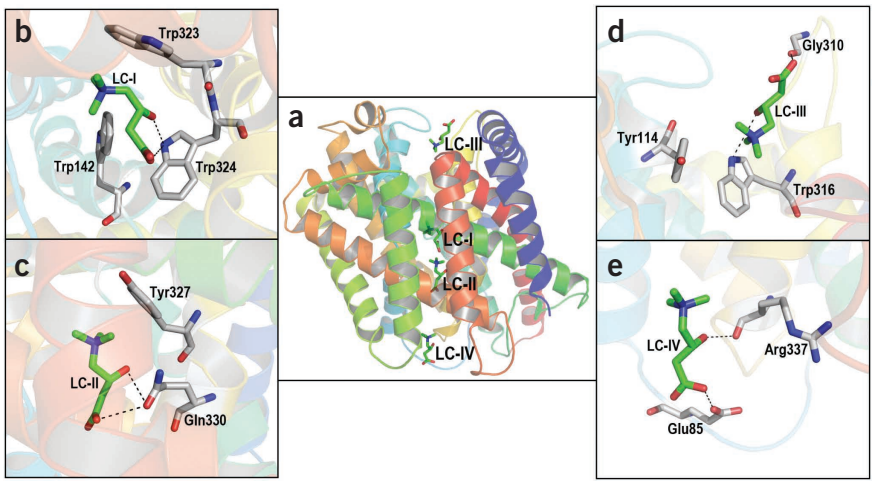

Figure 2 The substrate-binding sites. (**a**) Overview of CaiT with four bound substrate molecules. (**b**–**e**) Close-up images of the binding sites for L-carnitine molecules I (**b**), II (**c**), III (**d**) and IV (**e**), respectively.

of a cytoplasmic secondary binding site that has not been studied in detail. In a previous structural study on a LeuT–inhibitor complex[33], a competitive inhibitor molecule (Trp) was observed immediately above the primary binding site, and a periplasmic second binding site was also suggested (**Fig. 3b**). Subsequent structural studies indicated that this second binding site can also be occupied by a detergent molecule, and computational and biochemical analyses suggested that substrate binding the second site promoted a different state that would be essential for Na^+-coupled substrate transport[34,35]. Notably, LC-II is in the reciprocal position of the second binding site of LeuT. To assess the functional importance of this binding site, we mutated the two LC-II–interacting residues (Y327L and Q330L) and used the above mentioned proteoliposome-based transport assay to evaluate the impact of these mutations on the transport activity of CaiT. Our results indicate that the carnitine uptake of the mutants was markedly reduced (**Fig. 4**), supporting the existence of a previously undescribed cytoplasmic second substrate-binding site ($S_{in}1$).

Furthermore, structural comparison of BetP and CaiT provides clues on the association between the substrate-binding process at this site and the negotiation of the cytoplasmic barrier. In the 'occluded' state of BetP, residues Trp377 and Phe380, which correspond to Tyr327 and Gln330 in CaiT, respectively, are located immediately below the betaine substrate and prevent access to the cytosol (**Fig. 5**). However, in CaiT, Tyr327 and Gln330 coordinate with LC-II and concomitantly deviate to allow inward or outward permeation of the substrates (**Fig. 5b**), suggesting that the binding of LC-II is associated with the conformational rearrangements favoring the opening of the cytoplasmic gate. Moreover, the intracellular portions of TM3, TM4, TM8 and TM10 in CaiT show a deviation of ~2 Å from the corresponding portions of BetP, and the cytoplasmic loop that connects helices TM4 and TM5 (IL4) also shows remarkable conformational differences from the corresponding loop in BetP, suggesting that the rearrangements in these regions are coupled to the gating of the periplasmic barrier (**Fig. 5a**).

The third and fourth L-carnitine molecules

The third L-carnitine molecule, LC-III, is observed in a shallow cavity on the extracellular surface and is separated from LC-I by a 12-Å periplasmic barrier (**Fig. 3c**). LC-III forms hydrogen bonds with Gly310 (EL7) and Trp316 (TM8) and cation-π interactions with Trp316 (TM8) and Tyr114 (TM3e) (**Fig. 2d**). We induced mutations in Trp316 and Tyr114 and measured their transport activity. The results indicated that Y114L had a minor effect on the transport rate, whereas W316L reduced the transport rate by ~70% (**Fig. 4**). These results imply that substrate interaction with the aromatic residues at the top of the periplasmic barrier may be associated with the transport activity. Because CaiT shows a remarkable structural twofold symmetry and a core architecture similar to that of LeuT, we speculate that the outward-facing conformational state possesses a substrate-binding site located between LC-III and LC-I. This site ($S_{out}1$) is expected to be located at a position corresponding to that of the pockets of the second binding site in the outward-facing conformation of the LeuT complex (**Fig. 3a**,**b**). Structural comparison suggests that the aromatic residues at the center of the periplasmic barrier, such as residues Trp319 and Trp320, may be the components of such a binding site in CaiT (**Fig. 3c**).

In addition, we observed a fourth L-carnitine molecule, LC-IV, at the entrance of the intracellular vestibule. LC-IV was in contact with the Glu85 (IL2) and Arg337 (TM8) residues (**Fig. 2e**). However, the loose substrate–CaiT interactions and the large distance to the primary binding site (~15 Å) suggest that this site is a low-affinity, transiently occupied site.

DISCUSSION

In contrast to Na^+-coupled symporters, which possess a primary binding site and one or two Na^+-binding sites, the number and nature of substrate-binding sites in antiporters are less well known. This limitation has hindered the comprehension of the dynamic process of antiporter-mediated substrate translocation. Recently, the structures of three pH-dependent residue antiporters have been reported[29–31]. These antiporters have a common proposed binding site at the center of the protein, and this site was either occluded or exposed to one side of the membrane. This finding suggests that substrate exchange may follow the alternating-access transport mechanism. However, there is limited structural and functional information for the secondary binding sites.

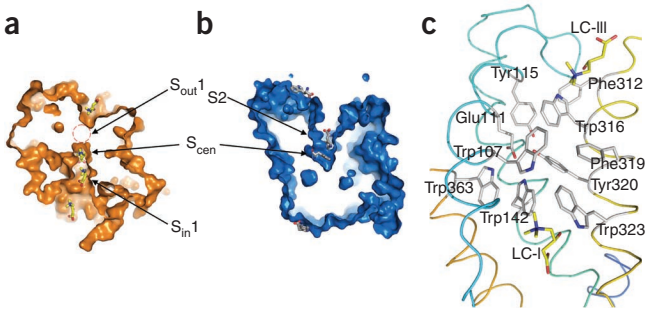

Figure 3 Comparison of the structures of CaiT and LeuT. (**a**,**b**) CaiT in complex with four L-carnitine molecules (**a**) and LeuT in complex with four tryptophan molecules (**b**) (PDB 3F3A), respectively. The L-carnitine and tryptophan molecules are represented in the form of sticks. The cytoplasmic binding site and potential periplasmic binding site of CaiT ($S_{out}1$), the pocket of the second binding site (S2) of LeuT and the primary binding sites (S_{cen}) for both CaiT and LeuT are indicated. (**c**) Close-up image of the periplasmic barrier.

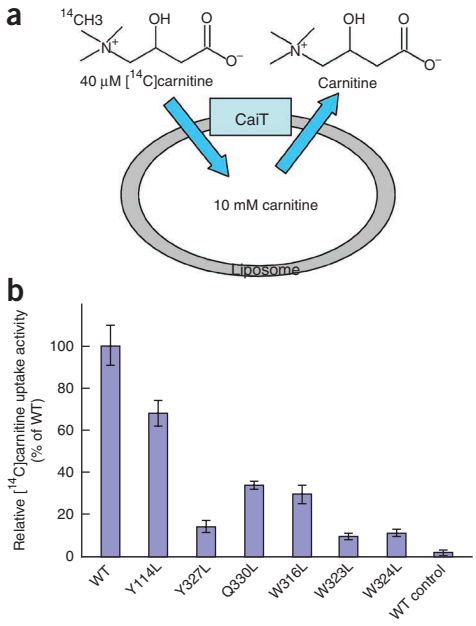

Figure 4 Characterization of the antiport activity for wild-type (WT) and mutant CaiT. (**a**) Depiction of the assay protocol. The uptake of 40 μM (external concentration) [^{14}C]carnitine into CaiT-reconstituted liposomes (5 μg mg^{-1} lipid; internal concentration of unlabeled carnitine, 10 mM) was monitored after 20 min of culture. (**b**) Summary of the results. The activity is expressed in terms of the percentage of WT (100%). Liposomes without internal unlabeled carnitine were considered as the WT control. The average values for three independent experiments are shown. Error bars, s.d. of triplicate experiments.

The structure of CaiT indicates the existence of secondary binding sites in addition to the central primary binding site, providing insights into the substrate-translocation process, particularly the translocation process in the absence of an ion gradient as the driving force. Sequence alignment suggested that a conserved Na^+-binding motif (Gly-X-Gly in TM3) for the Na^+-coupled symporters of the BCCT family is altered to Cys-Thr-Ser in CaiT (**Supplementary Fig. 2**). Moreover, in CaiT, two of the BetP residues that have been proposed to participate in the coordination of Na^+ (Ser468 in TM10 and Met310 in TM7)[21] are mutated to Leu422 and Ser263, respectively, and these mutations may account for the disruption of the Na^+-binding site in CaiT. These observations account for the previously obtained results showing that CaiT is a Na^+-independent exchanger, and they raise an interesting question regarding the process by which alternative isomerization between inward-facing and outward-facing orientations are promoted in the absence of an ion gradient. Our observations imply that functionally relevant secondary binding sites may exist on both sides of CaiT (termed $S_{in}1$ and $S_{out}1$, respectively). Moreover, we hypothesized that the opening and closing of these secondary binding sites may be coupled to the translocation of both precursor and product. For example, when the reaction starts from an 'apo inward-facing state', both the intracellular binding of the product to S_{cen} and the extracellular binding of the precursor to the top of the extracellular barrier (around residue Trp316) should aid the conformational rearrangements that facilitate the opening of $S_{out}1$, although the precursor may only have an accessory contribution in this scenario. However, further investigations will be required to confirm this speculation and decipher in-depth information about the 'driving force' behind antiport. We propose that the mechanistic insights obtained on the basis of our observations may be relevant in studies pertaining to other precursor/product antiporter mechanisms. However, further structural studies on the conformations of structurally homologous antiporters, particularly the outward-facing intermediate conformations, are required for a thorough understanding of the complete antiport process.

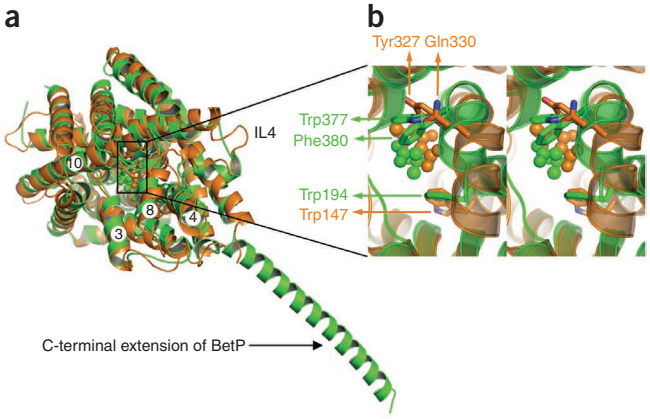

Figure 5 Structural superposition of CaiT (orange) with BetP (green). (**a**) An overall view from the cytoplasmic side. (**b**) A close-up image of the cytoplasmic gate. LC-I and betaine are shown as orange and green CPK models, respectively.

METHODS

Methods and any associated references are available in the online version of the paper at http://www.nature.com/nsmb/.

Accession codes. Protein Data Bank: Coordinates for CaiT have been deposited under the accession code 3HFX.

Note: Supplementary information is available on the Nature Structural & Molecular Biology website.

ACKNOWLEDGMENTS

We thank the staff at the European Synchrotron Radiation Facility in France, the Spring-8 (beamline BL41XU) in Japan and the Swiss Light Source (beamline X06SA) in Switzerland for help with data collection, J. Tang and Y.-B. Wang for technical support and J. Chen for discussions. This research was financially supported by the National Key Basic Research Program (grant numbers 2009CB918600, 2009CB918803), the National Natural Science Foundation of China (grant number 30721003), the National High Technology Research and Development Program of China (grant number 2006AA02A319) and the Knowledge Innovation Program of the Chinese Academy of Sciences (grant number KSCX2-YW-R-123).

AUTHOR CONTRIBUTIONS

L.T. performed expression, purification, crystallization and the crystal structure determination; L.B. and W.-h.W. contributed to vector construction and protein expression; L.B. performed the mutagenesis studies and transport activity measurements; T.J. and L.T. designed the research; T.J. supervised the work; L.T. and T.J. analyzed the results and wrote the paper.

COMPETING FINANCIAL INTERESTS

The authors declare no competing financial interests.

Published online at http://www.nature.com/nsmb/.
Reprints and permissions information is available online at http://npg.nature.com/reprintsandpermissions/.

1. Poolman, B. Precursor/product antiport in bacteria. *Mol. Microbiol.* **4**, 1629–1636 (1990).
2. Law, C.J., Maloney, P.C. & Wang, D.N. Ins and outs of major facilitator superfamily antiporters. *Annu. Rev. Microbiol.* **62**, 289–305 (2008).

3. Dierks, T., Riemer, E. & Krämer, R. Reaction mechanism of the reconstituted aspartate/glutamate carrier from bovine heart mitochondria. *Biochim. Biophys. Acta* **943**, 231–244 (1988).
4. Anantharam, V., Allison, M.J. & Maloney, P.C. Oxalate:formate exchange. The basis for energy coupling in *Oxalobacter*. *J. Biol. Chem.* **264**, 7244–7250 (1989).
5. Poolman, B., Royer, T.J., Mainzer, S.E. & Schmidt, B.F. Lactose transport system of *Streptococcus thermophilus*: a hybrid protein with homology to the melibiose carrier and enzyme III of phosphoenolpyruvate-dependent phosphotransferase systems. *J. Bacteriol.* **171**, 244–253 (1989).
6. Pebay-Peyroula, E. *et al.* Structure of mitochondrial ADP/ATP carrier in complex with carboxyatractyloside. *Nature* **426**, 39–44 (2003).
7. Jardetzky, O. Simple allosteric model for membrane pumps. *Nature* **211**, 969–970 (1966).
8. Jencks, W.P. The utilization of binding energy in coupled vectorial processes. *Adv. Enzymol.* **51**, 75–106 (1980).
9. Tanford, C. Mechanism of free energy coupling in active transport. *Annu. Rev. Biochem.* **52**, 379–409 (1983).
10. Fritz, I.B. & Yue, K.T. Effects of carnitine on acetyl-coA oxidation by heart muscle mitochondria. *Am. J. Physiol.* **206**, 531–535 (1964).
11. Treem, W.R., Stanley, C.A., Finegold, D.N., Hale, D.E. & Coates, P.M. Primary carnitine deficiency due to a failure of carnitine transport in kidney, muscle, and fibroblasts. *N. Engl. J. Med.* **319**, 1331–1336 (1988).
12. Nalecz, K.A., Miecz, D., Berezowski, V. & Cecchelli, R. Carnitine: transport and physiological functions in the brain. *Mol. Aspects Med.* **25**, 551–567 (2004).
13. Jung, K., Jung, H. & Kleber, H.P. Regulation of L-carnitine metabolism in *Escherichia coli*. *J. Basic Microbiol.* **27**, 131–137 (1987).
14. Kleber, H.P. Bacterial carnitine metabolism. *FEMS Microbiol. Lett.* **147**, 1–9 (1997).
15. Seim, H., Ezold, R., Kleber, H.P. & Strack, E. Metabolism of L-carnitine in enterobacteria. *Z. Allg. Mikrobiol.* **20**, 591–594 (1980).
16. Tamai, I. *et al.* Cloning and characterization of a novel human pH-dependent organic cation transporter, OCTN1. *FEBS Lett.* **419**, 107–111 (1997).
17. Wu, X., Prasad, P.D., Leibach, F.H. & Ganapathy, V. cDNA sequence, transport function, and genomic organization of human OCTN2, a new member of the organic cation transporter family. *Biochem. Biophys. Res. Commun.* **246**, 589–595 (1998).
18. Tamai, I. *et al.* Molecular and functional identification of sodium ion-dependent, high affinity human carnitine transporter OCTN2. *J. Biol. Chem.* **273**, 20378–20382 (1998).
19. Tein, I. Carnitine transport: pathophysiology and metabolism of known molecular defects. *J. Inherit. Metab. Dis.* **26**, 147–169 (2003).
20. Jung, H. *et al.* CaiT of *Escherichia coli*, a new transporter catalyzing L-carnitine/γ-butyrobetaine exchange. *J. Biol. Chem.* **277**, 39251–39258 (2002).
21. Peter, H., Burkovski, A. & Krämer, R. Isolation, characterization, and expression of the *Corynebacterium glutamicum betP* gene, encoding the transport system for the compatible solute glycine betaine. *J. Bacteriol.* **178**, 5229–5234 (1996).
22. Kappes, R.M., Kempf, B. & Bremer, E. Three transport systems for the osmoprotectant glycine betaine operate in *Bacillus subtilis*: characterization of OpuD. *J. Bacteriol.* **178**, 5071–5079 (1996).
23. Boscari, A., Mandon, K., Dupont, L., Poggi, M.C. & Le Rudulier, D. BetS is a major glycine betaine/proline betaine transporter required for early osmotic adjustment in *Sinorhizobium meliloti*. *J. Bacteriol.* **184**, 2654–2663 (2002).
24. Vinothkumar, K.R., Raunser, S., Jung, H. & Kühlbrandt, W. Oligomeric structure of the carnitine transporter CaiT from *Escherichia coli*. *J. Biol. Chem.* **281**, 4795–4801 (2006).
25. Ressl, S. *et al.* Molecular basis of transport and regulation in the Na^+/betaine symporter BetP. *Nature* **458**, 47–52 (2009).
26. Yamashita, A. *et al.* Crystal structure of a bacterial homologue of Na^+/Cl^-dependent neurotransmitter transporters. *Nature* **437**, 215–223 (2005).
27. Faham, S. *et al.* The crystal structure of a sodium galactose transporter reveals mechanistic insights into Na^+/sugar symport. *Science* **321**, 810–814 (2008).
28. Weyand, S. *et al.* Structure and molecular mechanism of a nucleobase-cation-symport-1 family transporter. *Science* **322**, 709–713 (2008).
29. Fang, Y. *et al.* Structure of a prokaryotic virtual proton pump at 3.2 Å resolution. *Nature* **460**, 1040–1043 (2009).
30. Gao, X. *et al.* Structure and mechanism of an amino acid antiporter. *Science* **324**, 1565–1568 (2009).
31. Shaffer, P.L., Goehring, A., Shankaranarayanan, A. & Gouaux, E. Structure and mechanism of a Na^+-independent amino acid transporter. *Science* **325**, 1010–1014 (2009).
32. Schiefner, A. *et al.* Cation-p interactions as determinants for binding of the compatible solutes betaine and proline betaine by the periplasmic ligand-binding protein ProX from *Escherichia coli*. *J. Biol. Chem.* **279**, 5588–5596 (2004).
33. Singh, S.K., Piscitelli, C.L., Yamashita, A. & Gouaux, E.A. Competitive inhibitor traps LeuT in an open-to-out conformation. *Science* **322**, 1655–1661 (2008).
34. Shi, L., Quick, M., Zhao, Y., Weinstein, H. & Javitch, J.A. The mechanism of a neurotransmitter: sodium symporter-inward release of Na^+ and substrate is triggered by substrate in a second binding site. *Mol. Cell* **30**, 667–677 (2008).
35. Quick, M. *et al.* Binding of an octylglucoside detergent molecule in the second substrate (S2) site of LeuT establishes an inhibitor-bound conformation. *Proc. Natl. Acad. Sci. USA* **106**, 5563–5568 (2009).
36. DeLano, W.L. The PyMOL Molecular Graphics System. (DeLano Scientific, San Carlos, California, USA, 2002) <http://www.pymol.org.>.

ONLINE METHODS

Expression and purification. We cloned the CaiT antiporter from *E. coli* into a pET28-derivative vector that included a C-terminal green fluorescent protein (GFP), a hexahistidine tag and a tobacco etch virus (TEV) protease cleavage site[37,38]. Sequencing showed that Met353 had been mutated to leucine. We produced the protein in *E. coli* C41 cells that had been cultured in Terrific broth after induction at an absorbance at 600 nm of 0.6 with 0.3 mM isopropyl-β-D-thiogalactopyranoside for 20 h at 18 °C. We isolated the cell membranes from the disrupted cells and solubilized them with 1% (w/v) *n*-dodecyl β-D-maltoside (DDM). We eluted GFP-CaiT from a metal ion affinity chromatography column using a buffer composed of 20 mM Tris-HCl (pH 8.0), 300 mM NaCl, 200 mM imidazole and 0.05% (w/v) DDM. After digestion with TEV, we loaded the protein onto a second metal ion affinity chromatography column to separate CaiT from TEV-His and GFP-His. We further purified the eluted CaiT protein on a Superdex 200 10/300 GL column (GE Healthcare) equilibrated with 50 mM HEPES-NaOH (pH 7.5), 150 mM NaCl and 0.03% (w/v) DDM. We concentrated CaiT to ~10 mg ml^{-1} using a 100-kDa Amicon Ultra-4 tube (Millipore) at 4 °C.

Crystallization. We grew CaiT crystals in the presence of L-carnitine using the hanging-drop vapor-diffusion method at 20 °C by mixing 10 mg ml^{-1} of the protein with a reservoir solution composed of 0.1 M HEPES-NaOH (pH 7.5), 20–26% (v/v) PEG-400, 0.1 M NaCl, 18 mM *N*-octyl-β-D-glucopyranoside and 5 mM L-carnitine. We obtained heavy atom derivatives by soaking the crystals in an artificial mother liquor containing 5 mM ethylmercurithiosalicylic acid and sodium salt ($C_9H_9HgNaO_2S$). Before freezing them in liquid nitrogen, we cryoprotected the crystals using a reservoir solution containing 30% (v/v) PEG-400, 0.020% (w/v) DDM and 10 mM *N*-octyl-β-D-glucopyranoside. The crystals belong to the $P6_3$ space group, with cell dimensions of $a = b = 134.2$ Å, $c = 85.1$ Å and $\alpha = \beta = 90°$, $\gamma = 120°$.

Structural determination. We collected X-ray diffraction datasets on a PILATUS 6M detector at the X06SA beamline at the Swiss Light Source, Paul Scherrer Institute, processed them with Mosfilm and scaled them using SCALA of the CCP4 suite[39]. We obtained the phases using the single anomalous dispersion method using a mercury peak-wavelength (1.0039 Å) dataset from a CaiT–L-carnitine crystal that had been soaked with mercury. We obtained heavy atom sites using the SHELX[40] software package and further refined them using the SHARP[41] algorithm. We calculated the initial experimental phases using SHARP and transferred them to the solvent-flattening procedures DM[42] in the same software package. We built a partial structure using PHENIX[43] at 3.15 Å and accomplished subsequent manual rebuilding using Coot[44]. We subjected the model to multiple rounds of refinement using REFMAC5[45] and CNS[46], with manual rebuilding in Coot between each round. The current model contains residues 12–504, nine mercury atoms and four L-carnitine molecules. The *R* factor and R_{free} are 26.2% and 28.1%, respectively. We checked the quality of the structure using PROCHECK[47]. The Ramachandran plot showed that 79.8% of residues lie within the most favored regions, with 20.2% in the additionally allowed and generously allowed regions; no residue was found in disallowed regions.

CaiT reconstitution and radioligand uptake assays. We prepared liposome using the protocol described previously[48]. We reconstituted purified CaiT into preformed liposomes that we prepared using chloroform-washed *E. coli* phospholipids in buffer A containing 50 mM HEPES (pH 7.5), 2 mM mercaptoethanol, 1% (v/v) glycerol, 0.5 mM EDTA,1 mM $MgSO_4$ and 10 mM carnitine. Before reconstitution, we made the liposomes into unilamellar vesicles by extruder and destabilized them by addition of 0.2% (w/v) DDM in buffer A. We then reconstituted purified CaiT at a protein-to-lipid ratio of 1:200 and incubated it at 4 °C for 1 h. We removed detergent by adding SM-2 Bio-Beads at ratios of wet weight bead to detergent of 40:1. After 2 h of incubation at 4 °C, we added fresh Bio-Beads, and we continued incubation overnight at 4 °C. After we removed Bio-Beads, we concentrated proteoliposomes by centrifugation at 180,000*g* for 1 h and destabilized them to 25 μg ml^{-1} protein with buffer B containing 50 mM HEPES (pH 7.5), 2 mM mercaptoethanol and 1 mM $MgSO_4$. For exchange experiments, we diluted aliquots (10 μl) of the proteoliposome suspension into 100 μl of buffer B. We added 2 μl L-[methyl-^{14}C]carnitine (53 Ci mol^{-1}) at a final concentration of 40 μM. We carried out transport assays at 25 °C and terminated them 20 min later by quenching of the reaction with 2.5 ml ice-cold buffer B and immediate filtration using Millipore GSTF 02500 filters (0.2-μm pore size). We performed all measurements a minimum of three times.

37. Drew, D., Lerch, M., Kunji, E., Slotboom, D.J. & de Gier, J.W. Optimization of membrane protein overexpression and purification using GFP fusions. *Nat. Methods* **3**, 303–313 (2006).
38. Collaborative Computational Project. Number 4. The CCP4 suite: programs for protein crystallography. *Acta Crystallogr. D Biol. Crystallogr.* **50**, 760–763 (1994).
39. Sheldrick, G.M. A short history of SHELX. *Acta Crystallogr. A* **64**, 112–122 (2008).
40. Vonrhein, C., Blanc, E., Roversi, P. & Bricogne, G. Automated structure solution with autoSHARP. *Methods Mol. Biol.* **364**, 215–230 (2007).
41. Terwilliger, T.C. *et al.* Iterative model building, structure refinement and density modification with the PHENIX AutoBuild wizard. *Acta Crystallogr. D Biol. Crystallogr.* **64**, 61–69 (2008).
42. Cowtan, K. An automated procedure for phase improvement by density modification. *Joint CCP4 and ESF-EACBM Newsletter on Protein Crystallography, DM* **31**, 34–38 (1994).
43. Emsley, P. & Cowtan, K. Coot: model-building tools for molecular graphics. *Acta Crystallogr. D Biol. Crystallogr.* **60**, 2126–2132 (2004).
44. Jones, T.A., Zou, J.Y., Cowan, S.W. & Kjeldgaard, M. Improved methods for building protein models in electron density maps and the location of errors in these models. *Acta Crystallogr. A* **47**, 110–119 (1991).
45. Murshudov, G.N., Vagin, A.A. & Dodson, E.J. Refinement of macromolecular structures by the maximum-likelihood method. *Acta Crystallogr. D Biol. Crystallogr.* **53**, 240–255 (1997).
46. Brünger, A.T. *et al.* Crystallography & NMR system: a new software suite for macromolecular structure determination. *Acta Crystallogr. D Biol. Crystallogr.* **54**, 905–921 (1998).
47. Laskowski, R.A., MacArthur, M.W., Moss, D.S. & Thornton, J.M. PROCHECK: a program to check the stereochemical quality of protein structures. *J. Appl. Crystallogr.* **26**, 283–291 (1993).
48. Jung, H., Tebbe, S., Schmid, R. & Jung, K. Unidirectional reconstitution and characterization of purified Na^+/proline transporter of *Escherichia coli*. *Biochemistry* **37**, 11083–11088 (1998).